

## Article

# Adsorption of Methylene Blue by Biosorption on Alkali-Treated *Solanum incanum*: Isotherms, Equilibrium and Mechanism

Hamza S. AL-Shehri <sup>1,†</sup> , Hamdah S. Alanazi <sup>2,†</sup>, Areej Mohammed Shaykhayn <sup>2</sup>, Lina Saad ALharbi <sup>2</sup>, Wedyan Saud Alnafaei <sup>2</sup>, Ali Q. Alorabi <sup>3</sup>, Ali S. Alkorbi <sup>4</sup> and Fahad A. Alharthi <sup>2,\*</sup>

<sup>1</sup> Chemistry Division, King Khaled Military Academy, SANG, Riyadh 11495, Saudi Arabia; alshehrih@kkma.edu.sa

<sup>2</sup> Department of Chemistry, College of Science, King Saud University, Riyadh 11451, Saudi Arabia; hsenzi@ksu.edu.sa (H.S.A.); areej\_shaykhayn@hotmail.com (A.M.S.); lenasaadx@outlook.com (L.S.A.); wedosmoon@gmail.com (W.S.A.)

<sup>3</sup> Chemistry Department, Faculty of Science, Al-Baha University, Al Baha 65731, Saudi Arabia; aalorabi@bu.edu.sa

<sup>4</sup> Empty Quarter Research Unit, Department of Chemistry, College of Science and Art in Sharurah, Najran University, Sharurah 68342, Saudi Arabia; assalem@nu.edu.sa

\* Correspondence: fharthi@ksu.edu.sa

† These authors contributed equally to this work.

**Abstract:** In this study, a new bio-adsorbent (NASIF) was successfully prepared via chemical activation of *Solanum incanum* (SI) with hydrogen peroxide and sodium hydroxide reagents as an inexpensive and effective adsorbent for the removal of methylene blue (MB) from aqueous media. The morphology of the NASIF adsorbent surface and the nature of the potential MB interactions were examined by Fourier transform infrared spectroscopy (FTIR) and scanning electron microscopy (SEM) micrograph. FTIR results suggested that carboxyl, carbonyl, and hydroxyl groups were involved in MB adsorption on the NASIF surface. EDX analysis confirmed the successful increase of oxygen-containing functional groups during the chemical activation. The influence of important factors was studied using the batch method. The results revealed that the maximum removal efficiency was 98% at contact time: 120 min; pH: 6.5, adsorbent dose: 40 mg; and temperature-25 °C. Isothermal behavior was evaluated using three non-linear isotherm models, Langmuir, Freundlich, and D-R isotherm. MB adsorption onto NASIF adsorbent followed the Langmuir isotherm model with maximum monolayer capacity (mg/g) at 25 °C. Meanwhile, the PSO kinetics model was found to be better than PFO kinetic model for describing the adsorption process using kinetic models. Based on the D-R model, the free energy ( $E$ , kJ mol<sup>-1</sup>) values were in the range of 0.090–0.1812 kJ mol<sup>-1</sup>, which indicated that the MB adsorption onto NASIF may belong to physical adsorption. The adsorption mechanism of MB onto NASIF adsorbent mainly includes electrostatic attraction,  $\pi$ - $\pi$  interaction,  $n$ - $\pi$  interaction, and H-bonding. The thermodynamic parameters revealed that the adsorption process was a feasibility, spontaneous and exothermic process. Finally, the result of the present work could provide strong evidence of the potential of NASIF adsorbent for eliminating MB from aqueous media.

**Keywords:** *Solanum incanum*; isotherm; adsorption; mechanism; methylene blue; exothermic



**Citation:** AL-Shehri, H.S.; Alanazi, H.S.; Shaykhayn, A.M.; ALharbi, L.S.; Alnafaei, W.S.; Alorabi, A.Q.; Alkorbi, A.S.; Alharthi, F.A. Adsorption of Methylene Blue by Biosorption on Alkali-Treated *Solanum incanum*: Isotherms, Equilibrium and Mechanism. *Sustainability* **2022**, *14*, 2644. <https://doi.org/10.3390/su14052644>

Academic Editors: Mohd Rafatullah and Masoom Raza Siddiqui

Received: 26 January 2022

Accepted: 16 February 2022

Published: 24 February 2022

**Publisher's Note:** MDPI stays neutral with regard to jurisdictional claims in published maps and institutional affiliations.



**Copyright:** © 2022 by the authors. Licensee MDPI, Basel, Switzerland. This article is an open access article distributed under the terms and conditions of the Creative Commons Attribution (CC BY) license (<https://creativecommons.org/licenses/by/4.0/>).

## 1. Introduction

Synthetic dyes are colored organic compounds released in wastewater from different industries such as cosmetics, textiles, rubber, printing, leather, plastics, paper, printing, and pharmaceutical, which cause a series of serious hazards to our water resources [1–3]. Methylene blue (MB), Rhodamine B (RB), Malachite green (MG), crystal violet (CV), etc., are water-soluble dyes and have stable physical and chemical properties, and are difficult to degrade [4]. Methylene blue (MB), known as methyl thioninium chloride, is a cationic thiazine dye with the molecular formula [C<sub>16</sub>H<sub>18</sub>N<sub>3</sub>SCl] [5]. It was widely used in many

industries, as mentioned above. Excessive release of MB dye causes abnormal colorization of surface water, hinders sunlight penetration, and reduces oxygen dissolution, which affects the photosynthesis of aquatic plants [6]. Therefore, dye molecules cause serious threats to the environmental system and health of humans that include carcinogenicity, dysfunction of the brain, kidneys, and liver [7–9]. A large amount of MB (more than  $7.0 \text{ mg kg}^{-1}$ ) can lead to mental disorders, high blood pressure, abdominal pain, and nausea [10]. Even low concentrations are very hazardous to the environment aquatic. Due to its harmfulness, it is important to remove these pollutants before their discharge into the environment.

Various approaches include photocatalytic degradation [11], ozone-based processes [12], membrane separation [13], free radical degradation [14], coagulation [15], chemical oxidation [16], and adsorption [17,18], etc. Among these approaches, adsorption has been considered as one of the most efficient methods for the removal of pollutants due to its low cost, high specific adsorption performance, economic method with efficient performance, high efficiency, and non-toxic adsorbents [19–21].

Various materials, either synthetic or natural, have been used for the elimination of MB dye from aqueous media. Materials with good adsorption performance, low cost, and natural affinity to pollutants are desired in the choice of adsorption materials, therefore, all these characteristics are found in bio-adsorbents. Additionally, biosorbents have numerous important characteristics such as eco-friendliness, biocompatibility, availability, and feasibility: hence their potential adsorption capacity to remove toxic pollutants from wastewater. Various biosorbents such as sugarcane Bagasse [22], *Terminalia catappa* (TC) shells [23], Guava leaves [24], *phoenix tree* leaf powder [25], *Platanus orientalis* leaves [26], *Rhus Coriaria* L [27], *Casuarina equisetifolia* pine [5], have been employed in the removal of methylene blue from aqueous solutions.

*Solanum incanum* is a perennial that grows naturally in southern Saudi Arabia and other countries (Tanzania, Kenya, Uganda, Australia, India, and Madagascar) [28]. The leaves and stems are yellowish-brown in color when ripe and they have small thorns, and the fruits are often 2–3 cm in diameter. *Solanum incanum* is used as medicine for managing hepatitis and reducing the risk of high blood pressure. *Solanum incanum* presents itself as a potential bio-adsorbent, owing to its wide availability in nature and with the objective of adding value to biomass in the polluted water treatment sector. To the best of our knowledge, there is no evidence from many studies on the potential use of activated *Solanum incanum* with  $\text{H}_2\text{O}_2$  as a bio-adsorbent in the treatment of wastewater.

The aim of the present work was to activate *Solanum incanum* leaves and flowers by chemical activation with  $\text{H}_2\text{O}_2$  and NaOH reagent to increase oxygen-containing functional groups on their surface and thus enhance the adsorptive properties. The activated adsorbents were characterized by SEM, EDX, elemental mapping, and FTIR. To the best of our knowledge, NASIF adsorbent has not been used yet for dye removal from aqueous media. The effects of contact time, adsorbent dose, initial MB concentration, and temperature on the removal of MB dye were achieved through the batch method. The kinetics and isotherm of MB adsorption on NASIF were investigated. The thermodynamic parameters have also been calculated. Additionally, the possible mechanisms for MB dye adsorption onto NASIF adsorbent were discussed.

## 2. Experiment

### 2.1. Chemicals and Instrumentation

All chemicals were used as received. Methylene blue (MB) and Rhodamine B (RB) dyes were obtained from Sigma Aldrich. Sodium hydroxide (NaOH), hydrochloric acid (HCl), and nitric acid ( $\text{HNO}_3$ ) were obtained from BDH, England. Deionized water was used in this work. The analysis of functional groups of UTSIF, NASIF, and MB-saturated NASIF were performed using Fourier transform infrared spectroscopy (Nicolet iS50 FTIR, Thermo Scientific). The surface morphological features of UTSIF, NASIF, and MB-saturated NASIF were analyzed with scanning electron microscopy, and Energy-dispersive X-ray

spectroscopy (Model JEM-2100F, JEOL, Japan). The MB and RB concentrations in the solutions were determined using a UV–Vis spectrophotometer (Perkin Elmer, 900T).

## 2.2. Chemical Treatment

For the present study, *Solanum incanum* leaves (SIL) and *Solanum incanum* flowers (SIF) were collected from Albaha region in Saudi Arabia. SIL and SIF materials were washed several times with deionized water to remove any adhering dirt. Then, the washed SIL and SIF were oven-dried at 100 °C for 24 h. Next, the dried SIL and SIF were crushed separately in the grinder to obtain fine powder. Chemical surface oxidation was carried out by immersing the SIF and SIL separately in 200 mL of 10% H<sub>2</sub>O<sub>2</sub> under stirring for 24 h at room temperature, which developed surface functionalities and enhanced the adsorptive properties [29,30]. After that, SIF and SIL powders were washed several times with deionized water and then filtered. The SIL and SIF were activated separately with a 1 M NaOH (200 mL) solution for 24 h. They were then washed off with deionized water, filtered, and dried in an oven at 50 °C for 24 h to obtain NaOH-activated *Solanum incanum* leaves (NASIL) adsorbent and NaOH-activated *Solanum incanum* leaves (NASIF) adsorbent.

## 2.3. Batch Adsorption Studies

Initial evaluation of the *Solanum incanum* flower (SIF), *Solanum incanum* leaves (SIL), NaOH-activated *Solanum incanum* flower (NASIF), NaOH-activated *Solanum incanum* flower (NASIL) adsorbent for adsorption of MB and RB dyes was conducted via batch adsorption experiments. The MB dye adsorption experiment performed was achieved under different operating parameters such as concentration (50–300 mg/L), various temperatures (25, 35, and 45 °C), reaction time (5–210 min), and adsorbent dosage (5–100 mg). A stock MB solution for the adsorption tests was prepared by dissolving MB in certain deionized water and then diluted to the desired MB concentrations. The original pH of the MB dye stock solution was approximately 6.5. All experimental solutions in this study were performed at pH 6.5 without any adjustments. A 40 mg sample of NASIF was charged into a conical flask containing 50 mL of MB (50 mg/L) and then the suspension was allowed to equilibrate using a shaker at room temperature for 100 min. After that, the suspension was separated by centrifuging at 5000 rpm for 10 min. Finally, the concentrations of MB and RB were measured using UV–Vis spectrophotometer at 663 nm and 556 nm, respectively. The removal efficiency of dyes and adsorption capacity of adsorbents were calculated by Equations (1) and (2), respectively.

$$\% \text{ adsorption} = \frac{C_0 - C_e}{C_0} \times 100 \quad (1)$$

$$q_e = (C_0 - C_e) \frac{V}{m} \quad (2)$$

where  $C_0$  is the concentration of the initial dyes;  $C_e$  (mg/L) is the equilibrium dye concentration;  $m$  (g) is the adsorbent mass and  $V$  (L) is the dye solution volume.

## 3. Results and Discussion

### 3.1. Bio-Adsorbent Characterization

The FTIR technique is an effective technique to identify functional groups of adsorbents. The FTIR spectra of UTSIF, NASIF, and MB-saturated NASIF are presented in Figure 1. The FTIR spectra of UTSIF powder show distinct peaks at 3438, 3013, 2931, 2852, 1741, 1624, 1459, 1375, 1265, 1157, and 1105 cm<sup>-1</sup>. In detail, the broad peak at 3438 cm<sup>-1</sup> is due to –OH stretching vibration of carboxylic acids and phenols in lignin, cellulose, and hemicellulose, suggesting the existence of hydroxyl and carboxylic acid on the surface of UTSIF and NASIF. This band increased in intensity with a small shift to 3443 cm<sup>-1</sup> after chemical activation [23,26,31]. The peaks at 3013, 2931, and 2852 cm<sup>-1</sup> were attributed to the stretching vibration of =C–H aromatic, asymmetric, and symmetric –C–H in methylene groups, respectively [32]. The strong peaks at 1741 and 1624 cm<sup>-1</sup> were due to the C=O (car-

bonyl, carboxyl) extending vibrations of keto-carbonyl gatherings and C=C bond [2,33,34]. After chemical modification (NASIF) the intensity of this peak increased. The peaks at  $1454\text{ cm}^{-1}$  were due to bending vibrations of the aliphatic C–H bonds or carboxylate asymmetric. This peak sharply increased in intensity and shifted to  $1462\text{ cm}^{-1}$ . In addition, a new peak appeared at  $1520\text{ cm}^{-1}$  due to an increase in the oxygen-containing functionalities on the surface of NASIF. The peaks at  $1375\text{ cm}^{-1}$ ,  $1265\text{ cm}^{-1}$ , and ( $1157\text{--}1105\text{ cm}^{-1}$ ) were assigned to C–N, C–O, C–O–C bonds [33,35]. A new peak that was observed at  $874\text{ cm}^{-1}$  and  $812\text{ cm}^{-1}$  (after chemical activation) was due to the out-of-plane bending of aromatic C–H [36,37]. Characteristic changes observed in the FTIR spectrum of NASIF after MB adsorption indicated that some peaks increased/decreased in intensity and shifted or disappeared. In detail, the intensity of the –OH and C=O groups shifted to  $3424\text{ cm}^{-1}$  and  $1735\text{ cm}^{-1}$  due to bending of –OH and C=O groups on the surface of NASIF with  $\text{R}(\text{CH}_3)_2\text{N}^+$  sites of MB by electrostatic interactions and H-bonding [35]. In addition, the intensity at  $1658\text{ cm}^{-1}$  increased and shifted to  $1606\text{ cm}^{-1}$ , which indicates  $\pi$ - $\pi$  interactions between the aromatic ring molecule in the NASIF adsorbent and the benzene ring in the MB molecule. Also, a peak of  $1520\text{ cm}^{-1}$  disappeared after MB adsorption onto NASIF surface adsorbent. Furthermore, the peak at  $874\text{ cm}^{-1}$  was increased in intensity and shifted to  $869\text{ cm}^{-1}$  due to H-bond formation between the N atoms of MB and H atoms of NASIF [38]. The observation supports interaction of MB with functional groups of NASIF via electrostatic, H-bonding,  $n$ - $\pi$  interactions, and  $\pi$ - $\pi$  interactions.

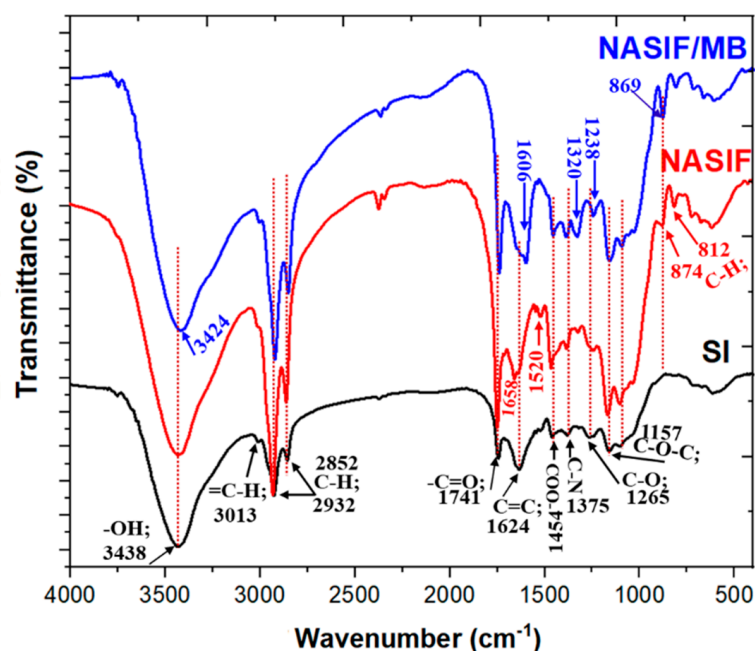


Figure 1. FTIR spectra of UTSIF, NASIF, and MB-saturated NASIF.

Figure 2 shows the morphology of UTSIF, NASIF, and MB-saturated NASIF. The surface of UTSIF shows a rough surface with pores and cracks (Figure 2a). After chemical activation, the porosity of NASIF surface increased (Figure 2b). After MB-saturated NASIF, the surface is covered and looks like a multilayered structure (Figure 2c). Thus, the SEM images of NASIF before and after MB-saturated NASIF display the differences in surface morphologies of these two adsorbents. The EDX of UTSIF adsorbent showed the existence of elements, mainly C (63.32%) and O (34.48%), with very trace elements of K and Ca (Table 1). The elemental mapping was carried out to identify the elements present in UTSIF, NASIF, and MB-saturated NASIF; therefore, the elemental mapping analysis in (Figure 3a) supports the presence of C, O, and other elements on the surface of the UTSIF adsorbent. After the chemical activation of UTSIF with  $\text{H}_2\text{O}_2$  and NaOH (Table 1), it was

observed that the weight% of oxygen increased to 44.08% while the weight% of carbon was reduced to 54.32%, indicating improved oxygen-containing functionalities on the surface of NASIF. The elemental mapping analysis confirms the distribution of elements after chemical activation; it was seen that the distribution of oxygen increased on the surface of the NASIF adsorbent (Figure 3b). After MB dye-saturated NASIF (Figure 4, a new peak of sulfide and nitrogen appeared with 0.81% and 0.02%, respectively (Table 1), indicating successful MB dye adsorption on NASIF adsorbent. The mapping results indicated the distribution of new elements (sulfide and nitrogen) over the NASIF surface (Figure 3c).

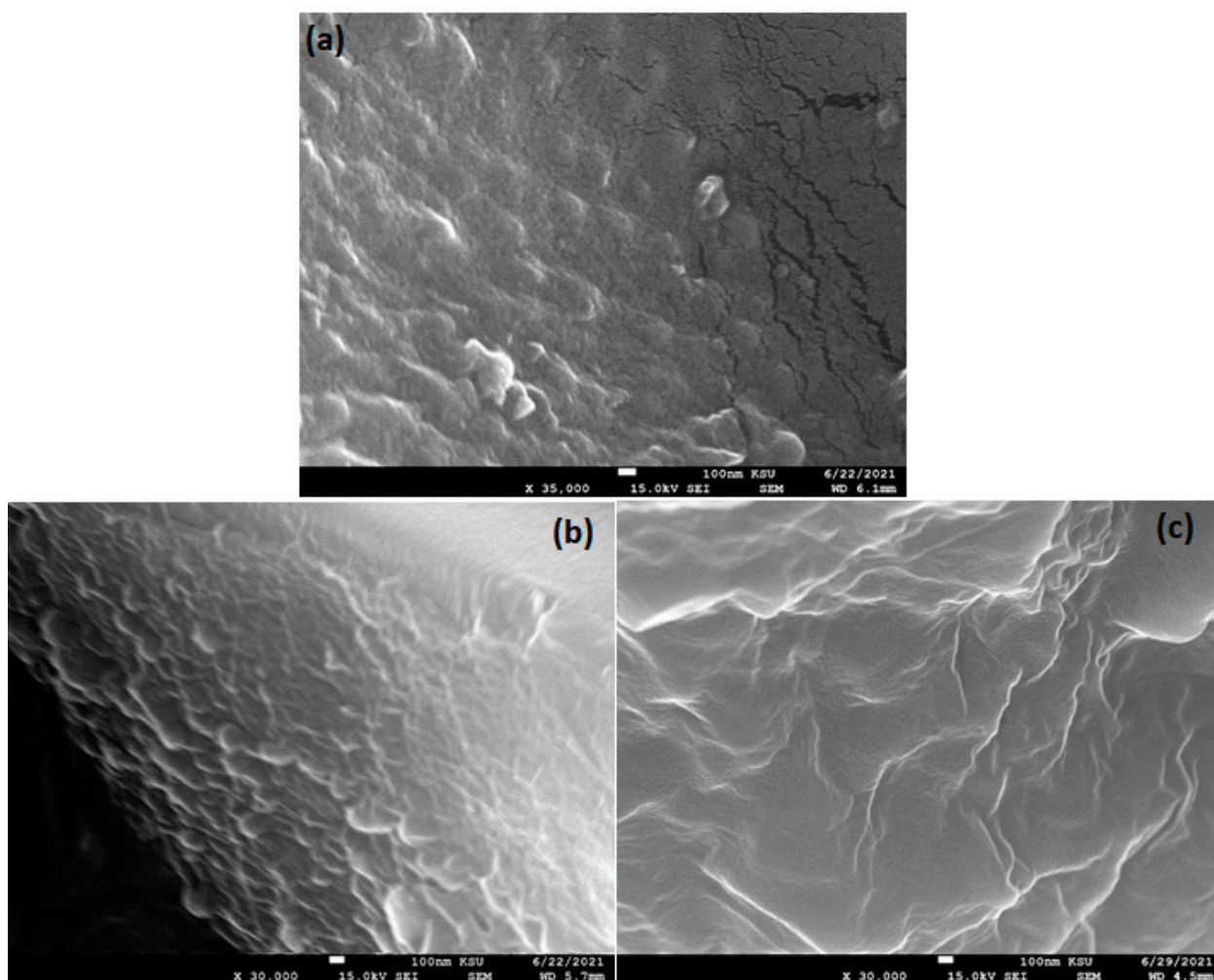


Figure 2. SEM images of (a) UTSIF, (b) NASIF, and (c) MB-saturated NASIF.

Table 1. Elemental analysis data.

Sample	Elemental Content (Wt.%)						
	C	O	Ca	K	Cl	S	N
UTSIF	63.14	34.48	0.76	1.36	0.25	-	-
NASIF	54.32	44.08	1.50	0.02	-	-	-
MB-saturated NASIF	66.97	32.14	-	-	0.07	0.81	0.02

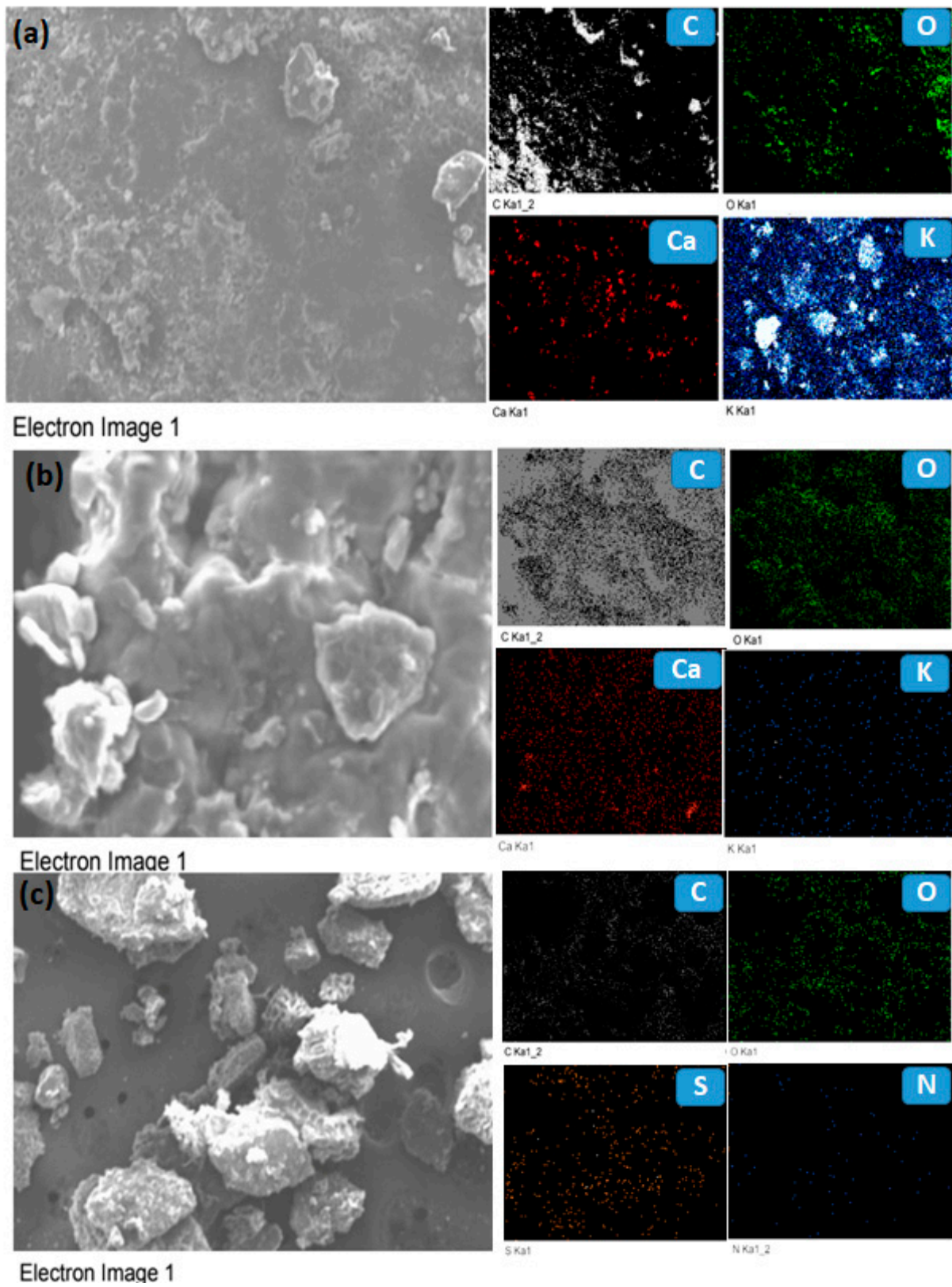


Figure 3. Elemental mapping analysis for (a) UTSIF, (b) NASIF, and (c) MB-saturated NASIF.

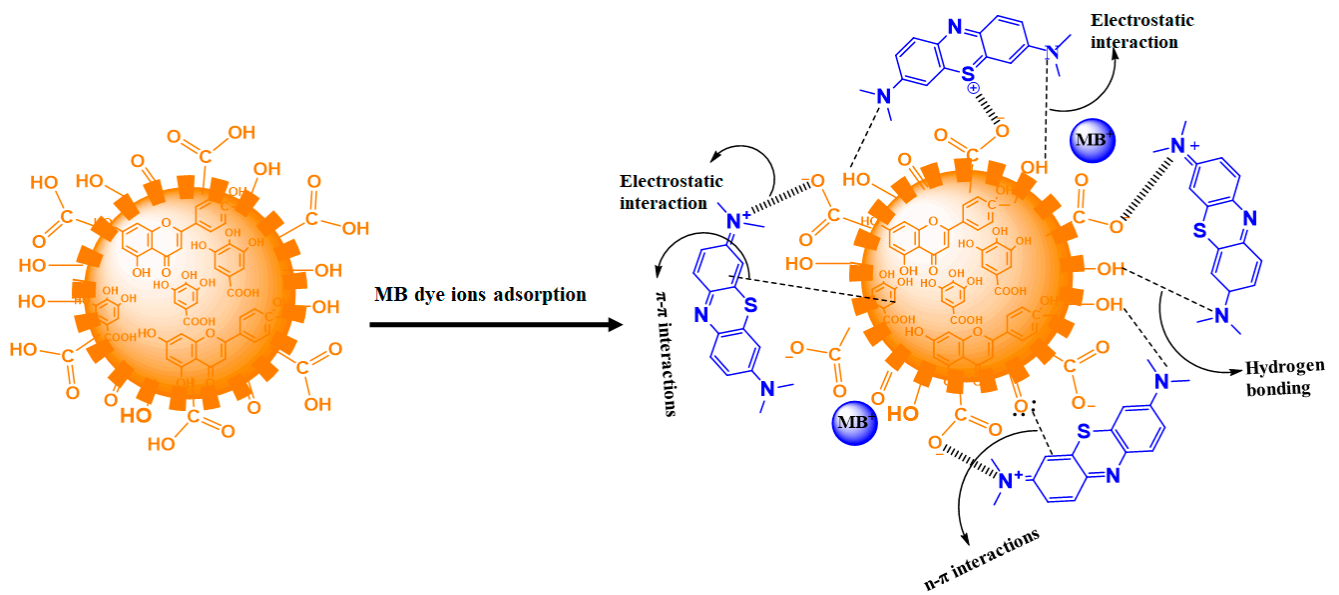


Figure 4. Mechanism of adsorption of MB using of NASIF adsorbent.

### 3.2. Adsorption Studies

#### 3.2.1. Selectivity Studies of Adsorbent

Four adsorbents—UTSIF, UTSIL, NASIF, and NASIL—for the adsorption of cationic dyes (MB and RB dyes) from aqueous solutions were tested under specific condition parameters (dose:  $C_0$ : 50 mg L<sup>-1</sup>; m: 40 mg; T: 25 °C; t: 24 h; pH: 6.5), as shown in Figure 5. The outcomes revealed that the four adsorbents show greater adsorption ability toward MB dye (95.6–99.0%) compared to RB dye (1.99–17.78%). In addition, the performance of NASIF and NASIL adsorbent was better than untreated UTSIF and UTSIL adsorbents toward the adsorption of MB dye. The high removal efficiencies of MB dye onto NASIF and NASIL adsorbents owes to the use of H<sub>2</sub>O<sub>2</sub> and NaOH as activation agents [39,40].

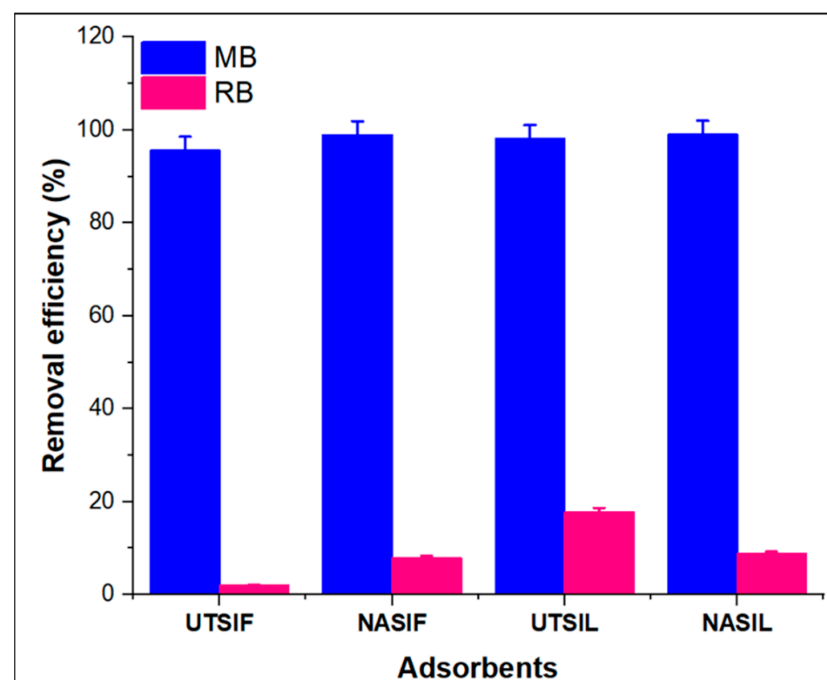


Figure 5. Selectivity studies of adsorbents toward MB and RB dyes.

### 3.2.2. Effect of Adsorbent Dose

The influence of adsorbent amount in the range from 0.05 mg to 0.1 mg on the adsorption process of MB using NASIF adsorbent has been examined as presented in Figure 6a. The result exhibited that the removal efficiency of MB dye increases significantly from 46.04% to 93.62% when the NASIF adsorbent mass rises from 0.01 g to 0.04 g. By improving the adsorbent amount, more adsorption active sites are available on the NASIF surface for interaction with MB molecules [9]. After this dose, no significant improvement in removal efficiency was observed. Oppositely, the adsorption capacity of NASIF adsorbent reduced significantly to 57.07 mg/g with the amount of NASIF adsorbent increasing to 0.04 g, due to the adsorption capacity being inversely proportional to the mass as per Equation (2) [41]. In addition, the rise in the amount of NASIF adsorbent may result in the aggregation of adsorbent and lead to some of the adsorption active sites overlapping, decreasing the adsorption capacity. These findings were similar to previous studies [2,42]. Thus, 40 mg of NASIF adsorbent was the optimum adsorbent dose in the subsequent studies.

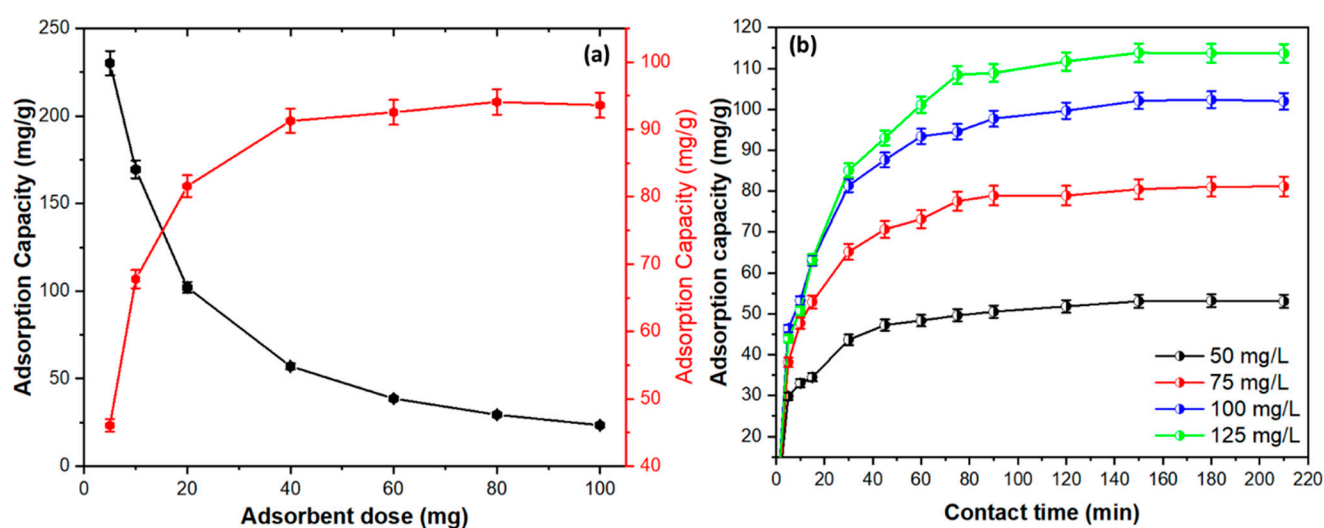


Figure 6. Effect of adsorbent dose (a), and contact time (b) on adsorption process.

### 3.2.3. Effect of Contact Time

The time-dependent adsorption capacity of NASIF was studied under different contact times (up to 210 min) and different MB concentrations (50, 75, 100, and 125 mg/L) as presented in Figure 6b (pH: 6.5; T: 25 °C; m: 0.04g). There is a rapid removal efficiency of MB dye (47.72%) within 5 min of the adsorption process due to the availability of abundant active sites on the surface of NASIF adsorbent. The adsorption capacities increased from 29.82 mg/g to 51.83 mg/g at 50 mg/L, 38.14 mg/g to 78.90 mg/g at 75 mg/L, 46.35 mg/g to 99.66 mg/g at 100 mg/L, and 43.92 mg/g to 111.63 mg/g at 125 mg/L as the contact time increased from 5 min to 120 min, respectively. After 120 min, the adsorption capacity became almost constant. Therefore, an optimum time of 120 min for MB was selected in the subsequent studies. A similar result has been detected in the adsorption of MB dye by different bio-adsorption materials [43,44].

### 3.2.4. Effect of Initial MB Concentration

The influence of various concentrations of MB dye (50 to 300 mg/L) on the adsorption process at various temperatures (25 to 45 °C) were investigated (pH: 6.5; m: 0.04 g; t: 120 min), as indicated in Figure 7a. According to Figure 6a, with the initial MB concentration increasing from 50 to 300 mg/L, adsorption capacities of NASIF adsorbent improved from 55.38 mg/g to 127.46 mg/g at 25 °C, 51.76 mg/g to 121.30 mg/g at 35 °C, and 46.54 mg/g to 112.90 mg/g at 45 °C. The increase in adsorption capacity with increasing initial MB concentrations was attributed to the driving force increases [45].

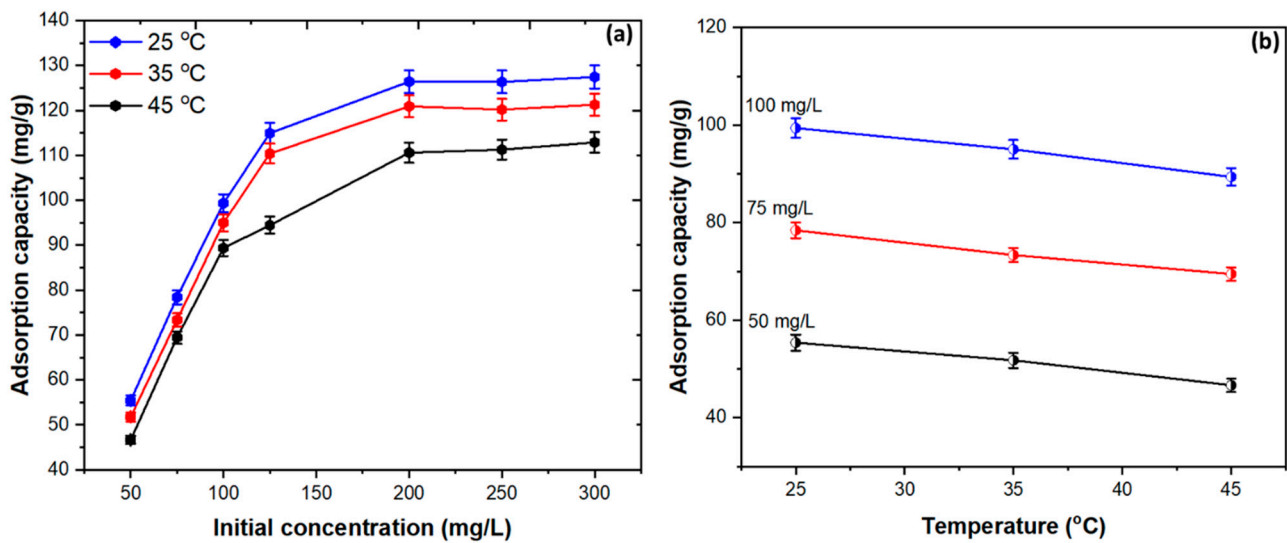


**Figure 7.** Effect of initial MB concentration (a), and temperature (b) on adsorption process.

### 3.2.5. Effect of Temperatures

The effect of various temperature (25, 35, 45 °C) on the adsorption process of MB using NASIF at various concentrations (50, 75, and 100 mg/L) under fixed condition parameters (pH: 6.5; T: 25 °C; m: 0.04 g; t: 120 min) adsorbent was studied as shown in Figure 7b. The results show that the adsorption ability of MB dye was reduced from 55.38 mg/g to 46.64 mg/g by increasing the test solution temperature from 25 °C to 45 °C at 50 mg/L, which shows that the adsorption of MB onto NASIF adsorbent is an exothermic process. This may be due to the destruction of binding sites between MB dye and NASIF adsorbent at 45 °C. This outcome is consistent with the literature reported in [41].

## 3.3. Adsorption Modeling

### 3.3.1. Isotherm Modeling

To study the adsorption behaviors of NASIF toward MB dye and mechanism adsorption, three nonlinear isotherm models (Langmuir Equation (3) [46], Freundlich Equation (4) [47], and D-R (Equations (5)–(7)) [48] isotherm models) were applied. The model parameters at different temperatures are presented in Table 2.

**Table 2.** Nonlinear isotherm models for MB adsorption on NASIF adsorbent.

Model	Temperature (K)		
	298	308	318
<b>Langmuir</b>			
$q_m$ , mg/g	135.24	132.35	124.11
$K_L$ (L/mg)	0.1262	0.0885	0.0266
$R^2$	0.98328	0.9484	0.94235
<b>Freundlich</b>			
$K_f$ , (mg/g) (L/mg) <sup>1/n</sup>	52.38	45.26136	36.03004
$n$	5.524	5.019	4.434
$R^2$	0.8073	0.7598	0.8016
<b>Dubinin–R</b>			
$q_s$ , mg/g	120.14	117.34	109.47
$K_{D-R}$ (mol <sup>2</sup> kJ <sup>-2</sup> )	15.235	33.422	61.739
$E$ (kJ mol <sup>-1</sup> )	0.1812	0.1223	0.0900
$R^2$	0.8312	0.8988	0.96173

$$q_e = \frac{q_m K_L C_e}{1 + K_L C_e} \quad (3)$$

$$q_e = K_F C_e^{1/n} \quad (4)$$

$$q_e = q_s e^{-K_{D-R} \varepsilon^2} \quad (5)$$

$$\varepsilon = RT \ln \left( 1 + \frac{1}{C_e} \right) \quad (6)$$

$$E = \frac{1}{\sqrt{2K_{D-R}}} \quad (7)$$

where,  $q_e$  (mg/g);  $q_m$  (mg/g);  $C_e$  (mg/L) represent the equilibrium adsorption capacity, maximum adsorption capacity at monolayer adsorption, and MB molecule concentration at equilibrium, respectively.  $K_L$  (L/mg);  $K_F$  (mg/g) (L/mg) $^{1/n}$ ;  $K_{DR}$  (mol $^2$ /kJ $^2$ ) represent the Langmuir constant, Freundlich constant, and D–R constant related to the adsorption energy, respectively. Variables  $n$ ;  $\varepsilon$ ;  $E$ (kJ/mol) represent the Freundlich isotherm intensity, Polanyi potential, and free energy, respectively. From Table 2 and Figure 8a–c and based on  $R^2$ , the adsorption data were observed to fit the Langmuir isotherm ( $R^2 = 0.98328$ ) compared to the other models (D–R ( $R^2 = 0.8312$ ), and Freundlich ( $R^2 = 0.8073$ )), indicating that the adsorption process can be described as monolayer adsorption and homogeneous surface with maximum monolayer capacity (135.24 mg/g). Based on Langmuir, the  $q_m$  values decreased with rising temperature, which emphasized that MB adsorption by NASIF is an exothermic reaction. Based on the D–R model, the adsorption free energy ( $E$ , kJ mol $^{-1}$ ) values were in the range of 0.090–0.1812 kJ mol $^{-1}$ , which indicated that MB adsorption onto NASIF may belong to physical adsorption [49]. Based on the Freundlich isotherm, the  $n$  values were in the range at different temperatures, which indicates a favorable adsorption process [50].

### 3.3.2. Kinetics Modeling

To understand the mechanism of MB adsorption onto NASIF and estimate the efficiency of the NASIF, two nonlinear kinetics models (pseudo-first-order (PFO) Equation (8) [51], and pseudo-second-order (PSO) Equation (9)) were applied.

$$q_t = q_e \left( 1 - e^{(-k_1 t)} \right) \quad (8)$$

$$q_t = \frac{q_e^2 k_2 t}{1 + q_e k_2 t} \quad (9)$$

where,  $k_1$  (1/min) and  $k_2$  (g/mg\*min) represent the PFO and PSO constant, respectively. The parameters with coefficient of determination ( $R^2$ ) values at various MB concentrations (50, 75, 100, and 125 mg/L) are summarized in Table 3. Based on  $R^2$  (Table 3 & Figure 8d), the MB adsorption onto NASIF was found to be more suited to the PSO kinetic model compared to PFO kinetic model at different MB concentrations (50, 75, 100, and 125 mg/L), which suggests the effect of chemical interactions in the adsorption process. In addition, the value of experimental  $q_e$  ( $q_{e_{exp}}$ ) for NASIF toward MB dye adsorption was 53.06 mg/g, which, being close to the calculated  $q_e$  ( $q_{e_{cal}} = 53.74$  mg/g at initial MB concentration (50 mg/L), confirmed the adsorption process followed by the PSO kinetics.

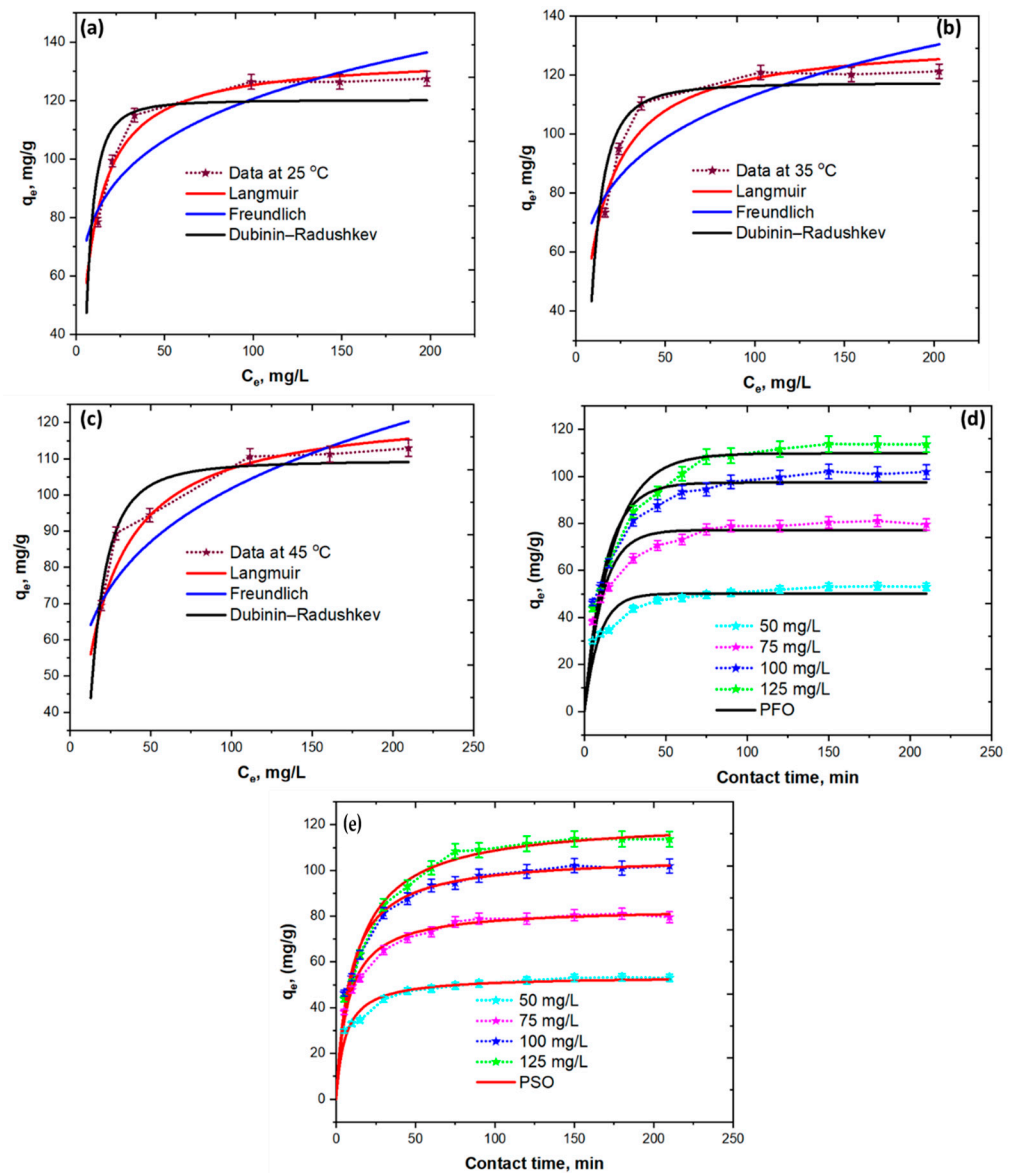


**Figure 8.** Nonlinear isotherm models at (a) 25 °C, (b) 35 °C, (c) 45 °C, and (d) Nonlinear kinetic models: pseudo-first-order and (e) pseudo-second-order for MB adsorption on NASIF.

**Table 3.** Nonlinear kinetics model for MB adsorption on NASIF adsorbent.

$C_0$ (mg/L)	$q_{e,exp}$ (mg/g)	Pseudo-First-Order			Pseudo-Second-Order		
		$q_{e1,cal}$ (mg/g)	$K_1$ (1/min)	$R^2$	$q_{e2,cal}$ (mg/g)	$K_2$ (g/mg-min)	$R^2$
50	53.06	50.1621	0.10976	0.93103	53.747	0.00319	0.9797
75	81.120	77.211	0.09167	0.95806	83.703	0.00161	0.9932
100	101.95	97.422	0.07849	0.95888	106.51	0.00106	0.9906
125	113.65	109.799	0.05836	0.96728	122.28	0.00065	0.9903

### 3.3.3. Thermodynamics Modeling

The thermodynamic analysis provides important insights into the adsorption nature and mechanism of adsorption. Therefore, the effect of solution temperature on MB adsorption onto NASIF was achieved through thermodynamic properties, as summarized in Table 4. Thermodynamic parameters including enthalpy change ( $\Delta H^\circ$ , kJ/mol) and

entropy change ( $\Delta S^\circ$ , kJ/mol·K) were calculated using van't Hoff equation Equation (11), while the free energy change ( $\Delta G^\circ$ , kJ/mol), was calculated using Equation (10) as follows:

$$\Delta G^\circ = -RT \ln K_c \quad (10)$$

$$\ln K_c = -\frac{\Delta H^\circ}{RT} + \frac{\Delta S^\circ}{R} \text{ (Van't Hoff equation)} \quad (11)$$

where T is the solution temperature (K); R is the universal gas constant (8.314 J/mol·K);  $K_c = q_e/c_e$  (L·g<sup>-1</sup>) represents the thermodynamic equilibrium constant [52]. Figure 9 demonstrates the relevant van't Hoff plots. From Table 4, a negative  $\Delta H^\circ$  suggests that the interaction of MB dye adsorbed by NASIF is exothermic, which is supported by the reducing adsorption of MB onto NASIF with the temperature rise. The values of  $\Delta H^\circ$  were lower than 40 kJ mol<sup>-1</sup>, further confirming that the MB adsorption onto NASIF belongs to the physisorption process [53]. The  $\Delta S$  value was negative, which indicates the decrease in randomness at the solid-solution interface between NASIF and MB solution. Negative  $\Delta G^\circ$  under different temperatures (25, 35, 45 °C) indicates a spontaneous adsorption process.

**Table 4.** Thermodynamics parameters for the adsorption of MB on NASIF adsorbent.

Concentration of CV Dye (mg/L)	(-) $\Delta H^\circ$ (kJ/mol)	(-) $\Delta S^\circ$ (J/mol.K)	(-) $\Delta G^\circ$ (kJ/mol)		
			298 K	308 K	318 K
50	38.34	109.68	5.63	4.59	3.44
75	22.97	61.80	4.59	3.86	3.37
100	17.13	44.30	3.910	3.52	3.02

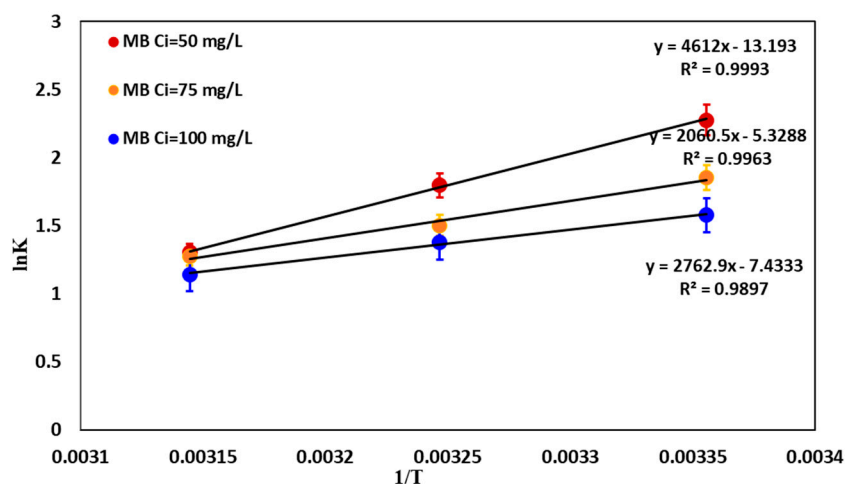


**Figure 9.** Adsorption thermodynamics.

### 3.4. Comparison with Other Adsorbents

The adsorption capacity of NASIF adsorbent toward the elimination of MB dye from aqueous solutions was compared to other bio-adsorbents, as presented in Table 5 [1,5,23,26,54–57]. The comparison indicates that the adsorption capacities of NASIF adsorbent were higher than those reported in many studies, due to increasing the oxygen-containing functionalities on the surface of NASIF by chemical activation with H<sub>2</sub>O<sub>2</sub>/NaOH reagents.

**Table 5.** Comparison of the maximum bio-adsorption capacities ( $q_m$ ) of NASIF for MB adsorption from different biomaterials.

Adsorbent	$q_m$ (mg/g)	Ref.
<i>Salix babylonica</i>	42.74	[1]
<i>Casuarina equisetifolia</i> pines	41.35	[5]
<i>Terminalia catappa</i> (TC) shells	88.62	[23]
<i>Platanus orientalis</i> leaves	114.94	[26]
<i>Ficus carica</i> bast	47.6	[54]
<i>Carica papaya</i> wood	32.25	[55]
<i>Pinus durangensis</i>	102	[56]
<i>Casuarina equisetifolia</i> pine/H <sub>2</sub> SO <sub>4</sub>	42.19	[57]
NASIF	135.24	This study

### 3.5. Adsorption Mechanism

The mechanism of MB dye adsorption onto NASIF was shown in Figure 1. To support the hypothesis given in Figure 1, FTIR analysis of the NASIF-loaded MB was conducted which suggest that the adsorption mechanism of MB on NASIF adsorbent mainly includes electrostatic attraction,  $n-\pi$  interaction,  $\pi-\pi$  interaction, and hydrogen bonding. There were distinctive changes observed in the FTIR spectrum of NASIF after MB adsorption indicated that some peaks increased/decreased in intensity and shifted or disappeared. In detail, the intensity of the  $-OH$  and  $C=O$  groups shifted from (3438 to 3424  $cm^{-1}$ ) and from (1741 to 1735  $cm^{-1}$ ), respectively. This shifting is due to the interactions of  $-OH$  and  $C=O$  groups on the surface of NASIF with  $R(CH_3)_2N^+$  sites of MB by electrostatic interactions and H-bonding [35]. In addition, the intensity at 1658  $cm^{-1}$  increased and shifted to 1606  $cm^{-1}$ , which indicates  $\pi-\pi$  interactions between the aromatic ring molecule in the NASIF adsorbent and the benzene ring in the MB molecule. Further, the peak at 874  $cm^{-1}$  increased in intensity and shifted to 869  $cm^{-1}$  due to H-bond formation between the N atoms of MB and H atoms of NASIF [38]. Also, a peak at 1520  $cm^{-1}$  disappeared after MB adsorption onto NASIF surface adsorbent, which suggests the formation of a  $n-\pi$  type interaction through donation of electron(s) from the oxygen in the carbonyl group present in the NASIF surface to the electron acceptors' aromatic rings in the MB dye [58,59]. These changes observed in the spectrum suggest interactions of MB dye with the functional groups of the NASIF in the adsorption process [21].

## 4. Conclusions

A new adsorbent, NaOH-activated *Solanum incanum* flower powder (NASIF), was successfully prepared by chemical activation method (H<sub>2</sub>O<sub>2</sub>/NaOH) as an inexpensive and effective adsorbent for the removal of methylene blue (MB) from aqueous media. The characterization of NASIF adsorbent was evaluated using FTIR and SEM, EDX, and elemental mapping. These technical results confirmed the adsorption of MB onto the NASIF adsorbent surface. The isothermal parameters indicated that the Langmuir model fit better than the Freundlich and D-R models, which confirmed the monolayer adsorption capacity of MB onto NASIF adsorbent. The MB adsorption onto NASIF adsorbent obeys the PSO kinetic model. The optimum conditions for NASIF adsorption of MB were contact time: 120 min; pH: 6.5, adsorbent dose: 40 mg; temperature-25 °C, with a maximum monolayer capacity of 135.24 mg/g. The D-R model revealed that the adsorption free energy ( $E$ ,  $kJ\ mol^{-1}$ ) values were in the range of 0.090–0.1812  $kJ\ mol^{-1}$ , which indicated that MB adsorption onto NASIF may belong to physical adsorption. The adsorption of MB onto the NASIF adsorbent surface occurred by electrostatic attraction,  $\pi-\pi$  interaction,  $n-\pi$  interaction, and H-bonding. Negative  $\Delta H$  and  $\Delta G$  values indicate that the adsorption process was exothermic in nature and spontaneous.

**Author Contributions:** F.A.A. and A.Q.A. played an important role in the project design and execution, while A.M.S., L.S.A. and W.S.A. carried out the experimental work. H.S.A.-S., H.S.A. and A.S.A. played a crucial role in the characterization and calculations of the results. F.A.A. and A.Q.A. compiled the data and prepared the manuscript. All authors have read and agreed to the published version of the manuscript.

**Funding:** We thank the King Saud University, Deanship of Scientific Research for funding this work through the research group No. RG-1441-305. We gratefully acknowledge the financial support by Albaha University (Project No. 1441/3) and are grateful to the Scientific Research.

**Conflicts of Interest:** The authors declare no conflict of interest.

## References

1. Kiwaan, H.A.; Mohamed, F.S.; El-Ghamaz, N.A.; Beshry, N.M.; El-Bindary, A.A. Experimental and electrical studies of zeolitic imidazolate framework-8 for the adsorption of different dyes. *J. Mol. Liq.* **2021**, *338*, 116670. [[CrossRef](#)]
2. Aldawsari, A.M.; Alsohaimi, I.H.; Al-Kahtani, A.A.; Alqadami, A.A.; Abdalla, Z.E.A.; Saleh, E.A.M. Adsorptive performance of aminoterephthalic acid modified oxidized activated carbon for malachite green dye: Mechanism, kinetic and thermodynamic studies. *Sep. Sci. Technol.* **2021**, *56*, 835–846. [[CrossRef](#)]
3. Alorabi, A.Q. Effective Removal of Malachite Green from Aqueous Solutions Using Magnetic Nanocomposite: Synthesis, Characterization, and Equilibrium Study. *Adsorpt. Sci. Technol.* **2021**, *2021*, 2359110. [[CrossRef](#)]
4. El-Bindary, M.A.; El-Desouky, M.G.; El-Bindary, A.A. Adsorption of industrial dye from aqueous solutions onto thermally treated green adsorbent: A complete batch system evaluation. *J. Mol. Liq.* **2022**, *346*, 117082. [[CrossRef](#)]
5. Chandarana, H.; Kumar, P.S.; Seenuvasan, M.; Kumar, M.A. Kinetics, equilibrium and thermodynamic investigations of methylene blue dye removal using *Casuarina equisetifolia* pines. *Chemosphere* **2021**, *285*, 131480. [[CrossRef](#)]
6. Fang, Y.; Liu, Q.; Zhu, S. Selective biosorption mechanism of methylene blue by a novel and reusable sugar beet pulp cellulose/sodium alginate/iron hydroxide composite hydrogel. *Int. J. Biol. Macromol.* **2021**, *188*, 993–1002. [[CrossRef](#)]
7. Alharthi, F.A.; Al-Zaqri, N.; el Marghany, A.; Alghamdi, A.A.; Alorabi, A.Q.; Baghdadi, N.; Al-Shehri, H.S.; Wahab, R.; Ahmad, N. Synthesis of nanocauliflower ZnO photocatalyst by potato waste and its photocatalytic efficiency against dye. *J. Mater. Sci. Mater. Electron.* **2020**, *31*, 11538–11547. [[CrossRef](#)]
8. Moghazy, R.M.; Labena, A.; Husien, S. Eco-friendly complementary biosorption process of methylene blue using micro-sized dried biosorbents of two macro-algal species (*Ulva fasciata* and *Sargassum dentifolium*): Full factorial design, equilibrium, and kinetic studies. *Int. J. Biol. Macromol.* **2019**, *134*, 330–343. [[CrossRef](#)]
9. Al-Wasidi, A.S.; AlZahrani, I.I.S.; Naglah, A.M.; El-Desouky, M.G.; Khalil, M.A.; El-Bindary, A.A.; El-Bindary, M.A. Effective Removal of Methylene Blue from Aqueous Solution Using Metal-Organic Framework; Modelling Analysis, Statistical Physics Treatment and DFT Calculations. *ChemistrySelect* **2021**, *6*, 11431–11447. [[CrossRef](#)]
10. Lyu, H.; Gao, B.; He, F.; Zimmerman, A.R.; Ding, C.; Tang, J.; Crittenden, J.C. Experimental and modeling investigations of ball-milled biochar for the removal of aqueous methylene blue. *Chem. Eng. J.* **2018**, *335*, 110–119. [[CrossRef](#)]
11. Soltani, N.; Saion, E.; Hussein, M.Z.; Erfani, M.; Abedini, A.; Bahmanrokh, G.; Navasery, M.; Vaziri, P. Visible light-induced degradation of methylene blue in the presence of photocatalytic ZnS and CdS nanoparticles. *Int. J. Mol. Sci.* **2012**, *13*, 12242–12258. [[CrossRef](#)] [[PubMed](#)]
12. Zhang, J.; Lee, K.-H.; Cui, L.; Jeong, T. Degradation of methylene blue in aqueous solution by ozone-based processes. *J. Ind. Eng. Chem.* **2009**, *15*, 185–189. [[CrossRef](#)]
13. Karisma, D.; Febrianto, G.; Mangindaan, D. Removal of dyes from textile wastewater by using nanofiltration polyetherimide membrane. In *IOP Conference Series: Earth and Environmental Science*; IOP Publishing: Bristol, UK, 2017; p. 12012.
14. Xiao, Z.; Li, Y.; Fan, L.; Wang, Y.; Li, L. Degradation of organic dyes by peroxymonosulfate activated with water-stable iron-based metal organic frameworks. *J. Colloid Interface Sci.* **2021**, *589*, 298–307. [[CrossRef](#)] [[PubMed](#)]
15. Guibal, E.; Roussy, J. Coagulation and flocculation of dye-containing solutions using a biopolymer (Chitosan). *React. Funct. Polym.* **2007**, *67*, 33–42. [[CrossRef](#)]
16. Dutta, K.; Mukhopadhyay, S.; Bhattacharjee, S.; Chaudhuri, B. Chemical oxidation of methylene blue using a Fenton-like reaction. *J. Hazard. Mater.* **2001**, *84*, 57–71. [[CrossRef](#)]
17. Alqadami, A.A.; Naushad, M.; Alothman, Z.A.; Ahamad, T. Adsorptive performance of MOF nanocomposite for methylene blue and malachite green dyes: Kinetics, isotherm and mechanism. *J. Environ. Manag.* **2018**, *223*, 29–36. [[CrossRef](#)]
18. Kiwaan, H.A.; Mohamed, F.S.; El-Bindary, A.A.; El-Ghamaz, N.A.; Abo-Yassin, H.R.; El-Bindary, M.A. Synthesis, identification and application of metal organic framework for removal of industrial cationic dyes. *J. Mol. Liq.* **2021**, *342*, 117435. [[CrossRef](#)]
19. Alorabi, A.Q.; Hassan, M.S.; Azizi, M.; Mohsen, Z.S.A.; Alzahrani, W.A.M.; Alzahrani, K.A.M.; Alghamdi, S.M.O.; Alharthi, F.F.M. Corrigendum to “Fe<sub>3</sub>O<sub>4</sub>-CuO-activated carbon composite as an efficient adsorbent for bromophenol blue dye removal from aqueous solutions”. [*Arab. J. Chem.* **13**(11) (2020) 8080–8091]. *Arab. J. Chem.* **2022**, *15*, 103508. [[CrossRef](#)]
20. Alorabi, A.Q.; Hassan, M.S.; Alam, M.M.; Zabin, S.A.; Alsenani, N.I.; Baghdadi, N.E. Natural Clay as a Low-Cost Adsorbent for Crystal Violet Dye Removal and Antimicrobial Activity. *Nanomaterials* **2021**, *11*, 2789. [[CrossRef](#)]

21. Alorabi, A.Q.; Alharthi, F.A.; Azizi, M.; Al-Zaqri, N.; El-Marghany, A.; Abdelshafeek, K.A. Removal of Lead(II) from Synthetic Wastewater by *Lavandula pubescens* Decne Biosorbent: Insight into Composition–Adsorption Relationship. *Appl. Sci.* **2020**, *10*, 7450. [[CrossRef](#)]
22. Bagotia, N.; Sharma, A.K.; Kumar, S. A review on modified sugarcane bagasse biosorbent for removal of dyes. *Chemosphere* **2021**, *268*, 129309. [[CrossRef](#)]
23. Hevira, L.; Zilfa; Rahmayeni; Ighalo, J.O.; Aziz, H.; Zein, R. Terminalia catappa shell as low-cost biosorbent for the removal of methylene blue from aqueous solutions. *J. Ind. Eng. Chem.* **2021**, *97*, 188–199. [[CrossRef](#)]
24. RGAikwad, W.; Kinldy, S.A.M. Studies on auramine dye adsorption on psidium guava leaves. *Korean J. Chem. Eng.* **2009**, *26*, 102–107. [[CrossRef](#)]
25. Han, R.; Wang, Y.; Zhao, X.; Wang, Y.; Xie, F.; Cheng, J.; Tang, M. Adsorption of methylene blue by phoenix tree leaf powder in a fixed-bed column: Experiments and prediction of breakthrough curves. *Desalination* **2009**, *245*, 284–297. [[CrossRef](#)]
26. Peydayesh, M.; Rahbar-Kelishami, A. Adsorption of methylene blue onto *Platanus orientalis* leaf powder: Kinetic, equilibrium and thermodynamic studies. *J. Ind. Eng. Chem.* **2015**, *21*, 1014–1019. [[CrossRef](#)]
27. Dülger, Ö.; Turak, F.; Turhan, K.; Özgür, M. Sumac Leaves as a Novel Low-Cost Adsorbent for Removal of Basic Dye from Aqueous Solution. *ISRN Anal. Chem.* **2013**, *2013*, 210470. [[CrossRef](#)]
28. Kaunda, J.S.; Zhang, Y.-J. Chemical constituents from the fruits of *Solanum incanum* L. *Biochem. Syst. Ecol.* **2020**, *90*, 104031. [[CrossRef](#)]
29. Xue, Y.; Gao, B.; Yao, Y.; Inyang, M.; Zhang, M.; Zimmerman, A.R.; Ro, K.S. Hydrogen peroxide modification enhances the ability of biochar (hydrochar) produced from hydrothermal carbonization of peanut hull to remove aqueous heavy metals: Batch and column tests. *Chem. Eng. J.* **2012**, *200–202*, 673–680. [[CrossRef](#)]
30. Huff, M.D.; Lee, J.W. Biochar-surface oxygenation with hydrogen peroxide. *J. Environ. Manag.* **2016**, *165*, 17–21. [[CrossRef](#)]
31. Alhumaimess, M.S.; Alshohaimi, I.H.; Alqadami, A.A.; Khan, M.A.; Kamel, M.M.; Aldosari, O.; Siddiqui, M.R.; Hamedelnieel, A.E. Recyclable glutaraldehyde cross-linked polymeric tannin to sequester hexavalent uranium from aqueous solution. *J. Mol. Liq.* **2019**, *281*, 29–38. [[CrossRef](#)]
32. Naushad, M.; Alqadami, A.A.; Ahamad, T. Removal of Cd(II) ion from aqueous environment using triaminotriethoxysilane grafted oxidized activated carbon synthesized via activation and subsequent silanization. *Environ. Technol. Innov.* **2020**, *18*, 100686. [[CrossRef](#)]
33. Üner, O. Hydrogen storage capacity and methylene blue adsorption performance of activated carbon produced from *Arundo donax*. *Mater. Chem. Phys.* **2019**, *237*, 121858. [[CrossRef](#)]
34. Alshareef, S.A.; Otero, M.; Alanazi, H.S.; Siddiqui, M.R.; Khan, M.A.; Allothman, Z.A. Upcycling olive oil cake through wet torrefaction to produce hydrochar for water decontamination. *Chem. Eng. Res. Des.* **2021**, *170*, 13–22. [[CrossRef](#)]
35. Köseoğlu, E.; Akmil-Başar, C. Preparation, structural evaluation and adsorptive properties of activated carbon from agricultural waste biomass. *Adv. Powder Technol.* **2015**, *26*, 811–818. [[CrossRef](#)]
36. Gao, P.; Zhou, Y.; Meng, F.; Zhang, Y.; Liu, Z.; Zhang, W.; Xue, G. Preparation and characterization of hydrochar from waste eucalyptus bark by hydrothermal carbonization. *Energy* **2016**, *97*, 238–245. [[CrossRef](#)]
37. Kang, S.; Li, X.; Fan, J.; Chang, J. Characterization of hydrochars produced by hydrothermal carbonization of lignin, cellulose, D-xylose, and wood meal. *Ind. Eng. Chem. Res.* **2012**, *51*, 9023–9031. [[CrossRef](#)]
38. Tural, B.; Ertaş, E.; Enez, B.; Fincan, S.A.; Tural, S. Preparation and characterization of a novel magnetic biosorbent functionalized with biomass of *Bacillus Subtilis*: Kinetic and isotherm studies of biosorption processes in the removal of Methylene Blue. *J. Environ. Chem. Eng.* **2017**, *5*, 4795–4802. [[CrossRef](#)]
39. Guo, Y.; Yang, S.; Yu, K.; Zhao, J.; Wang, Z.; Xu, H. The preparation and mechanism studies of rice husk based porous carbon. *Mater. Chem. Phys.* **2002**, *74*, 320–323. [[CrossRef](#)]
40. le Van, K.; Thi, T.T.L. Activated carbon derived from rice husk by NaOH activation and its application in supercapacitor. *Prog. Nat. Sci. Mater. Int.* **2014**, *24*, 191–198. [[CrossRef](#)]
41. Do, T.H.; Nguyen, V.T.; Dung, N.Q.; Chu, M.N.; van Kiet, D.; Ngan, T.T.K.; van Tan, L. Study on methylene blue adsorption of activated carbon made from *Moringa oleifera* leaf. *Mater. Today Proc.* **2021**, *38*, 3405–3413. [[CrossRef](#)]
42. Alqadami, A.A.; Naushad, M.; Ahamad, T.; Algamdi, M.; Alshahrani, A.; Uslu, H.; Shukla, S.K. Removal of highly toxic Cd(II) metal ions from aqueous medium using magnetic nanocomposite: Adsorption kinetics, isotherm and thermodynamics. *Desalin. Water Treat.* **2020**, *181*, 355–361. [[CrossRef](#)]
43. Danish, M.; Ahmad, T.; Nadhari, W.; Ahmad, M.; Khanday, W.A.; Ziyang, L.; Pin, Z. Optimization of banana trunk-activated carbon production for methylene blue-contaminated water treatment. *Appl. Water Sci.* **2018**, *8*, 9. [[CrossRef](#)]
44. Rashid, J.; Tehreem, F.; Rehman, A.; Kumar, R. Synthesis using natural functionalization of activated carbon from pumpkin peels for decolourization of aqueous methylene blue. *Sci. Total Environ.* **2019**, *671*, 369–376. [[CrossRef](#)] [[PubMed](#)]
45. Tharaneedhar, V.; Kumar, P.S.; Saravanan, A.; Ravikumar, C.; Jaikumar, V. Prediction and interpretation of adsorption parameters for the sequestration of methylene blue dye from aqueous solution using microwave assisted corncob activated carbon. *Sustain. Mater. Technol.* **2017**, *11*, 1–11. [[CrossRef](#)]
46. Wallis, A.; Dollard, M.F. Local and global factors in work stress—The Australian dairy farming exemplar. *Scand. J. Work. Environ. Health* **2008**, *34*, 66–74.
47. Freundlich, H. Über die Adsorption in Lösungen. *Z. Phys. Chem.* **1907**, *57U*, 385. [[CrossRef](#)]

48. Dubinin, M.M. Equation of the characteristic curve of activated charcoal. *Chem. Zentr.* **1947**, *1*, 857.
49. Alqadami, A.A.; Naushad, M.; Othman, Z.A.A.L.; Alsuhybani, M.; Algamdi, M. Excellent adsorptive performance of a new nanocomposite for removal of toxic Pb(II) from aqueous environment: Adsorption mechanism and modeling analysis. *J. Hazard. Mater.* **2020**, *389*, 121896. [[CrossRef](#)]
50. Alqadami, A.A.; Khan, M.A.; Siddiqui, M.R.; Alothman, Z.A.; Sumbul, S. A facile approach to develop industrial waste encapsulated cryogenic alginate beads to sequester toxic bivalent heavy metals. *J. King Saud Univ. Sci.* **2020**, *32*, 1444–1450. [[CrossRef](#)]
51. Lagergren, S. About the theory of so-called adsorption of soluble substances. *Handlingar* **1898**, *24*, 1–39.
52. Lee, L.Y.; Gan, S.; Tan, M.S.Y.; Lim, S.S.; Lee, X.J.; Lam, Y.F. Effective removal of Acid Blue 113 dye using overripe *Cucumis sativus* peel as an eco-friendly biosorbent from agricultural residue. *J. Clean. Prod.* **2016**, *113*, 194–203. [[CrossRef](#)]
53. Khan, M.A.; Wabaidur, S.M.; Siddiqui, M.R.; Alqadami, A.A.; Khan, A.H. Silico-manganese fumes waste encapsulated cryogenic alginate beads for aqueous environment de-colorization. *J. Clean. Prod.* **2020**, *244*, 118867. [[CrossRef](#)]
54. Pathania, D.; Sharma, S.; Singh, P. Removal of methylene blue by adsorption onto activated carbon developed from *Ficus carica* bast. *Arab. J. Chem.* **2017**, *10*, S1445–S1451. [[CrossRef](#)]
55. Rangabhashiyam, S.; Lata, S.; Balasubramanian, P. Biosorption characteristics of methylene blue and malachite green from simulated wastewater onto *Carica papaya* wood biosorbent. *Surfaces Interfaces* **2018**, *10*, 197–215. [[CrossRef](#)]
56. Salazar-Rabago, J.J.; Leyva-Ramos, R.; Rivera-Utrilla, J.; Ocampo-Perez, R.; Cerino-Cordova, F.J. Biosorption mechanism of Methylene Blue from aqueous solution onto White Pine (*Pinus durangensis*) sawdust: Effect of operating conditions. *Sustain. Environ. Res.* **2017**, *27*, 32–40. [[CrossRef](#)]
57. Chandarana, H.; Suganya, S.; Madhava, A.K. Surface functionalized *Casuarina equisetifolia* pine powder for the removal of hetero-polyaromatic dye: Characteristics and adsorption. *Int. J. Environ. Anal. Chem.* **2020**, 1–15. [[CrossRef](#)]
58. Tang, Y.; Zhao, Y.; Lin, T.; Li, Y.; Zhou, R.; Peng, Y. Adsorption performance and mechanism of methylene blue by H<sub>3</sub>PO<sub>4</sub>-modified corn stalks. *J. Environ. Chem. Eng.* **2019**, *7*, 103398. [[CrossRef](#)]
59. Dinh, V.-P.; Huynh, T.-D.-T.; Le, H.M.; Nguyen, V.-D.; Dao, V.-A.; Hung, N.Q.; Tuyen, L.A.; Lee, S.; Yi, J.; Nguyen, T.D.; et al. Insight into the adsorption mechanisms of methylene blue and chromium(iii) from aqueous solution onto pomelo fruit peel. *RSC Adv.* **2019**, *9*, 25847–25860. [[CrossRef](#)]